

Prethermal stability of eigenstates under high frequency Floquet driving

Nicholas O'Dea,¹ Fiona Burnell,² Anushya Chandran,³ and Vedika Khemani¹

¹*Department of Physics, Stanford University, Stanford, CA 94305, USA*

²*Department of Physics, University of Minnesota Twin Cities, MN 55455, USA*

³*Department of Physics, Boston University, MA 02215, USA*

Systems subject to high-frequency driving exhibit Floquet prethermalization, that is, they heat exponentially slowly on a time scale that is large in the drive frequency, $\tau_h \sim \exp(\omega)$. Nonetheless, local observables can decay much faster via energy conserving processes, which are expected to cause a rapid decay in the fidelity of an initial state. Here we show instead that the fidelities of *eigenstates* of the time-averaged Hamiltonian, H_0 , display an exponentially long lifetime over a wide range of frequencies – even as generic initial states decay rapidly. When H_0 has quantum scars, or highly excited-eigenstates of low entanglement, this leads to long-lived non-thermal behavior of local observables in certain initial states. We present a two-channel theory describing the fidelity decay time τ_f : the *interzone* channel causes fidelity decay through energy absorption i.e. coupling across Floquet zones, and ties τ_f to the slow heating time scale, while the *intrazone* channel causes hybridization between states in the same Floquet zone. Our work informs the robustness of experimental approaches for using Floquet engineering to generate interesting many-body Hamiltonians, with and without scars.

Introduction— Periodic driving is a powerful tool to engineer exotic phases of many-body quantum systems. High-frequency Floquet drives can be used to stabilize effective Hamiltonians displaying a variety of equilibrium phases, or to create intrinsically non-equilibrium phases [1–10]. In the absence of many-body localization, the drive ultimately thermalizes the system to a featureless infinite-temperature state, which is the maximum entropy state in the absence of conservation laws [11, 12]. Nevertheless, there are bounds which show that the time-scale for heating can be made exponentially slow, so that $\tau_h \geq \exp(\omega/J)$, where J is a typical instantaneous local energy scale in the problem, and ω is the drive frequency [13–23]. Intuitively, the system requires $O(\omega/J)$ local rearrangements to absorb one quantum (ω) of energy. In the prethermal regime, $t \lesssim \tau_h$, the local dynamics is well-described by a quasi-local effective Hamiltonian, H_{eff} , which can be constructed order-by-order in a high-frequency expansion in $(1/\omega)$. The leading order term is the time-averaged Hamiltonian, H_0 . Numerous experiments have used periodic driving to engineer interesting H_0 's, e.g. with artificial gauge fields [24–27] or with quantum scars [28].

In this Letter, we investigate the stability of individual eigenstates of the time-averaged Hamiltonian H_0 under dynamics generated by the full time-dependent Hamiltonian $H(t)$. In the prethermal regime, $t \lesssim \tau_h$, H_{eff} is approximately conserved, and hence eigenstates of H_{eff} are expected to show slow dynamics. However, the practical target for Floquet engineering approaches are eigenstates of H_0 (as opposed to H_{eff}), for which the current literature does not give any guarantee of slow dynamics. We therefore consider how long a generic (possibly highly excited) eigenstate $|\psi\rangle$ of H_0 can “survive” under the dynamics of the full time evolution generated by $H(t)$. To quantify this, we study the time-dependent fidelity [30, 31]:

$$F(t) = |\langle \psi | U(t) | \psi \rangle|^2. \quad (1)$$

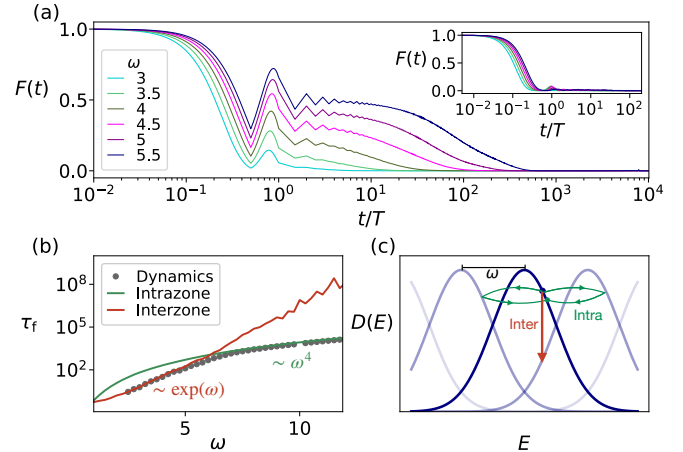


FIG. 1. (a) The fidelity against time, $F(t)$, for a highly-excited eigenstate of H_0 at zero energy density driven by $H(t)$ (Eq. (2)). The fidelity is long-lived, and the lifetime shows strong frequency dependence. Inset shows the rapid decay of $F(t)$ for a zero energy density product state $|00\dots0\rangle$ (not an eigenstate of H_0). (b) Comparison of the numerically extracted fidelity decay timescale τ_f with the interzone and intrazone FGR predictions [29], demonstrating the crossover between the two regimes. The data is for the same eigenstate as in (a). (c) Schematic showing the density of states of H_0 vs energy E in a replicated zone scheme. The arrows show the dominant interzone and intrazone processes causing fidelity decay. Parameters: model in Eq. (8), $L = 14$, $F(t)$ evaluated at stroboscopic times after one period.

where $U(t)$ is the full Floquet time evolution operator.

Since the difference between H_0 and H_{eff} is $O(1/\omega)$, a naive Fermi Golden Rule (FGR) calculation predicts a decay timescale for the fidelity $\sim \omega^2$; this is parametrically shorter than the heating time $\tau_h \sim \exp(\omega/J)$ (beyond which H_{eff} ceases to be a good description). Surprisingly, as shown in Fig. 1(a), we find that eigenstates of H_0 survive for much longer over a wide range of frequen-

cies. The fidelity curves are roughly linearly spaced on a semi-log scale, pointing to an *exponential-in-frequency* time-scale for the fidelity decay, similar to τ_h . These long lifetimes are only observed for eigenstates of H_0 ; in contrast, the inset shows that the fidelity of a generic state rapidly decays over just one driving period. In [29], we show heating and fidelity data for both generic initial states and eigenstates of H_0 ; while all states show exponentially slow heating, only eigenstates of H_0 show long-lived fidelity.

To explain these unexpectedly long fidelity lifetimes, we analyze two channels that contribute to fidelity decay (see Fig. 1b): an “intrazone channel” incorporating the effects of higher-order terms in H_{eff} , and an “interzone channel” that causes heating. Intrazone processes are well-captured by a perturbative high frequency expansion (solid green line), while heating processes, which are non-perturbative in ω , are well-captured by second-order time-dependent perturbation theory (TDPT) (solid red line). *Both* channels yield decay timescales which are parametrically longer than the naively expected $\tau_f \sim \omega^2$.

A striking feature of Fig. 1(b) is that for a wide range of frequencies, the interzone channel dominates and gives $\tau_f \sim \exp(\omega)$. At larger frequencies, the intrazone channel determines the observed $O(\omega^4)$ lifetime. In practice, however, the exponentially large interzone fidelity decay timescale might be all that is empirically accessible, since real experiments have to be careful to not excite high-energy degrees of freedom that lie outside the scope of the original isolated system, such as higher bands in lattice models. Similarly, in numerics the finite energy bandwidth limits the range of accessible frequencies.

Our results are of particular interest to approaches using high-frequency driving to engineer H_0 ’s with quantum many-body scars [32–36]. While fidelities of many-body eigenstates are not generally experimentally accessible, scarred models have eigenstates for which the expectation values of local observables are strikingly different than for typical eigenstates of the same energy. Initial states with large overlaps on these outlier eigenstates can be experimentally prepared; the dynamics of local observables then inherit the stability of eigenstates, as shown in Fig. 3. Interestingly, we find that scarred eigenstates survive for *even longer* than non-scarred eigenstates of H_0 at similar energies.

Two channels for fidelity decay— We consider periodically driven systems in d spatial dimensions of the form

$$H(t) = H_0 + \lambda V g(t), \quad (2)$$

where $g(t) = g(t + T)$ is a periodic function with period $T = 2\pi/\omega$ which time-averages to zero. The linear dimension is L , and the initial state $|\psi\rangle$ is an eigenstate of H_0 . We consider short-ranged models $H_0 = \sum_i h_i, V = \sum_i V_i$, where h_i, V_i have support near site i and set the local energy scale to J . The stroboscopic dynamics is governed by the Floquet unitary $U_F = \mathcal{T} \exp\left(-i \int_0^T H(t) dt\right)$ which time-evolves the sys-

tem by one period and defines the Floquet Hamiltonian H_F via $U_F \equiv e^{-iH_F T}$. In the prethermal regime $t \lesssim \tau_h$, the stroboscopic dynamics is well-described by a quasi-local effective Hamiltonian [14, 16]

$$H_{\text{eff}} = H_0 + \sum_{m=1}^n \frac{H^{(m)}}{\omega^m} \quad (3)$$

where $H^{(m)}$ is the m^{th} order term in the high-frequency Magnus expansion, and the series is truncated at an optimal order $n \propto \omega/J$. Because H_{eff} is almost conserved, its eigenstates are theoretically guaranteed to show slow dynamics up to times $t \lesssim \tau_h$. However, H_{eff} does not include the effects of heating, as the heating rate $\tau_h^{-1} \sim e^{-\omega/J}$ is non-perturbative in powers of $(1/\omega)$. The process of Floquet heating entails the system resonantly exchanging energy with the drive in quanta of size $\sim \omega$, which is visualized as a drive mediated coupling across “Floquet zones” representing copies of the eigenspectrum of H_0 displaced by integer multiples of ω (Fig. 1(c)).

Thus, the quasi-local and approximately conserved H_{eff} describes the dynamics induced by the drive within a Floquet zone (intrazone), while the heating process is described by coupling between zones (interzone). The latter is reflected in the non-perturbative, non-local character of H_F : the difference between $U_F = e^{-iH_F T}$ and $e^{-iH_{\text{eff}} T}$ is the heating process across Floquet zones visible on times $t > \tau_h$.

To find compact, analytical forms for the fidelity decay rate in terms of matrix elements in the H_0 eigenbasis, we use time-dependent perturbation theory (TDPT) and the assumptions of Fermi’s golden rule (FGR) [29]. The Dyson series for the time-evolution operator $U_I(t)$ in the interaction picture leads to a perturbative expansion of $\log(F(t))$ in powers of λ :

$$\begin{aligned} \log(F(t)) &= 2 \text{Re}[\log(\langle \psi | U_I(t) | \psi \rangle)] \\ &= \sum_{n=0}^{\infty} \lambda^n G^{(n)}(t) \end{aligned} \quad (4)$$

The time evolved state $U(t)|\psi\rangle$ generically deviates from $|\psi\rangle$ on all sites; the fidelity is consequently exponentially small in L^d , so that its logarithm has an extensive series expansion. Note that (i) a log fidelity rate $\propto L^d$ is consistent with a system size independent decay rate of local observables [29], and (ii) the series in Eq. (4) contains both perturbative and non-perturbative contributions in $\frac{1}{\omega}$.

The leading contributions to the intrazone and interzone processes are respectively derived from the $O(\lambda^2)$ and $O(\lambda^4)$ terms of the $\log(F(t))$ TDPT series in Eq. (4). Expressions for general drives are provided in [29] which, for a sinusoidal drive, $g(t) = \sin(\omega t)$ take the form:

$$R_{\psi}^{\text{inter}} = \frac{\pi \lambda^2}{2} (\mathcal{A}_{\psi}^V(\omega) + \mathcal{A}_{\psi}^V(-\omega)) \quad (5)$$

$$R_{\psi}^{\text{intra}} = \frac{\pi \lambda^4}{8\omega^4} \mathcal{A}_{\psi}^{[V, [H_0, V]]}(0) \quad (6)$$

Here, $\mathcal{A}_\psi^O(\omega) = \sum_n |O_{\psi n}|^2 \delta((E_n - E_\psi) - \omega)$ denotes the spectral function of an operator O in an eigenstate $|\psi\rangle$ of H_0 . When O is an extensive sum of local operators, the spectral function is exponentially suppressed at large frequencies, $\mathcal{A}_\psi^O(\omega) \sim L^d e^{-|\omega|/J}$.¹

The interzone rate R_ψ^{inter} is exponentially suppressed in frequency via the spectral function $\mathcal{A}_\psi^V(\pm\omega)$. The leading process contributing to R_ψ^{inter} couples the state ψ to states in neighboring Floquet zones (Fig. 1(c)). This happens at first order in the driving, $O(\lambda)$, which squares to give an $O(\lambda^2)$ contribution to $F(t)$. Interzone coupling is also responsible for energy absorption in multiples of the frequency ω ; indeed, for $g(t) = \sin(\omega t)$, the heating rate is [29],

$$R_\psi^{\text{heat}} = \frac{\pi\lambda^2}{2} \omega (\mathcal{A}_\psi^V(\omega) - \mathcal{A}_\psi^V(-\omega)), \quad (7)$$

which involves the same spectral functions as in Eq. (5).

In contrast, the leading contribution to the intrazone rate R_ψ^{intra} is a second-order process which couples ψ to a nearby-in-energy state ψ_f in the same Floquet zone, mediated by a virtual hop to a state ψ_k in a neighboring Floquet zone (Fig. 1(c)). This occurs at $O(\lambda^2)$, which squares to give an $O(\lambda^4)$ contribution to $F(t)$. This process involves terms of the form $\sum_k \lambda^2 \langle \psi_f | V | \psi_k \rangle \langle \psi_k | V | \psi \rangle / (E_k - E_f + \omega)$ when ψ_k belongs to the zone shifted by $+\omega$ and E_k is the eigenenergy of ψ_k which is an eigenstate of H_0 . Due to the decay of spectral functions with energy differences, the matrix elements are largest for processes where $E_\psi \approx E_k \approx E_f$ (Fig. 1(c)), which gives a $1/\omega$ contribution in the denominator. Upon squaring, the intrazone rate is thus naively expected to scale as $\frac{1}{\omega^2}$. However, in TDPT a cancellation between terms involving virtual transitions to neighboring Floquet zones, i.e. spectra shifted by $\pm\omega$ (Fig. 1c), leads instead to a dependence scaling as $\frac{1}{\omega^4}$ [29] and controlled by the spectral function of $[V, [H_0, V]]$. Heuristically:

$$\begin{aligned} & \sum_k \frac{\lambda^2 \langle \psi_f | V | \psi_k \rangle \langle \psi_k | V | \psi \rangle}{(E_k - E_f + \omega)} + \frac{\lambda^2 \langle \psi_f | V | \psi_k \rangle \langle \psi_k | V | \psi \rangle}{(E_k - E_f - \omega)} \\ & \approx \frac{2\lambda^2}{\omega^2} \sum_k \langle \psi_f | V | \psi_k \rangle \langle \psi_k | V | \psi \rangle (E_k - E_f) \\ & \approx \frac{\lambda^2}{\omega^2} \langle \psi_f | [V, [H_0, V]] | \psi \rangle \end{aligned}$$

where we have kept the leading $1/\omega$ contribution and used $E_\psi \approx E_k \approx E_f$. This squares to give an $O(\lambda^4/\omega^4)$ leading contribution to R_ψ^{intra} . The cancellation above relies on the fact that the matrix elements coupling ψ

to states in neighboring zones are guaranteed to be the same, since the zones are just shifted copies of the spectrum of H_0 .

The intrazone contribution in Eq. (6), which is perturbative in $\frac{1}{\omega}$, can also be obtained from TDPT applied to the high-frequency Floquet-Magnus expansion in Eq. (3). In this latter method, we truncate the high-frequency expansion of the Floquet-Magnus Hamiltonian to order $O(\frac{1}{\omega^2})$, and treat the dynamics as a quench to this time-independent Hamiltonian at $t = 0$ via Eq. (4) [29]. In the Floquet-Magnus treatment, the $1/\omega^4$ dependence arises because the spectral function of $H^{(1)} \propto [H_0, V]$ in Eq. (3) has a soft gap, $\mathcal{A}_\psi^{H^{(1)}}(0) = 0$, such that $H^{(1)}$ does not contribute to the FGR rate. The next order term $H^{(2)} \propto [V, [H_0, V]]$ is $O(\frac{1}{\omega^2})$, and contributes the observed $O(\frac{1}{\omega^4})$ rate via FGR. Note that drives with multiple non-commuting terms, for example $V_A \cos(\omega t) + V_B \cos(\omega t + \phi)$ can induce a term $H^{(1)} \propto \frac{[V_A, V_B]}{\omega}$ in the first order of the Floquet-Magnus expansion, which can lead to an asymptotically larger intrazone rate $O(\frac{1}{\omega^2})$. Nevertheless, there can remain an intermediate frequency window in which the decay is dominated by interzone processes and τ_f increases exponentially with frequency.

We expect the larger rate to set the timescale for the fidelity decay, $\tau_f \sim \frac{1}{R^{\text{inter}} + R^{\text{intra}}}$. Thus at large frequency, there is a crossover from interzone to intrazone dominated fidelity decay. The crossover frequency is $O(1)$ but can be made parametrically large by reducing λ/J [29]. In general, weak, high-frequency driving is most amenable to observing prethermal stability for eigenstates of H_0 .

Numerics— We turn to testing our two-channel picture through exact numerics on spin chains. Consider the following spin-1 scarred H_0 and driving protocol:

$$\begin{aligned} H_0 &= \sum_i h_i \\ h_i &= S_i^x S_{i+1}^x + S_i^y S_{i+1}^y + .1 (S_i^x S_{i+3}^x + S_i^y S_{i+3}^y + (S_i^z)^2) \\ H(t) &= H_0 + \lambda \text{Sgn}(\sin(\omega t)) \sum_i S_i^x \end{aligned} \quad (8)$$

Numerics are performed with $\lambda = 0.5$.

Without the drive, H_0 is the spin-1 XY model which conserves total z -magnetization and has a tower of quantum scarred eigenstates [37–39], $\left(\sum_{i=1}^L (-1)^i (S_i^+)^2 \right)^n | - - - \dots - - \rangle$ for $n = 0, 1, \dots, L$. There is one such scar state in each $S^z = -L, -L+2, \dots, L$ sector, with quasi-momentum 0 or π depending on whether n is even or odd. The scar states have energy density .1, close to the infinite temperature energy density of .06. The scar states are not eigenstates in the presence of the S^x drive.

We implement a box drive with multiple harmonics. The resulting interzone and intrazone fidelity decay rates are obtained using the same methods as for Eqs. (5) and (6) and give qualitatively similar results [29]. Fig. 1(a)

¹ In one dimension, $\mathcal{A}_\psi^O(\omega)$ is bounded above by a value of order $Le^{-|\omega| \log(|\omega|)/J}$ [14]. The extra suppression from the $\log(\omega)$ in the argument of the exponential does not significantly change any results.

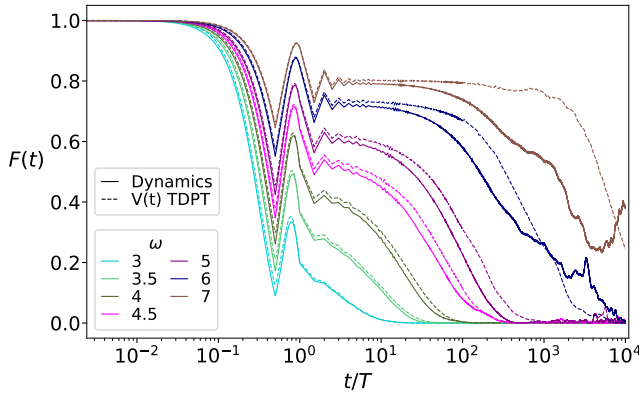


FIG. 2. Comparison of numerically exact fidelity dynamics under $H(t)$ (solid line) with 2nd-order TDPT (dotted line) for different drive frequencies ω . TDPT predicts the entire curve $F(t)$ well for $3 \leq \omega \lesssim 5$. Parameters: $L = 14$, eigenstate of H_0 in the $S^z = 0$, momentum $k = 0$, inversion antisymmetric, spin-flip antisymmetric sector next to the scar state in energy.

(discussed previously) plots $F(t)$ for a zero energy density eigenstate. Fig. 1(b) compares the numerically extracted decay timescale τ_f to the two-channel FGR predictions. We discuss the numerical extraction of the two-channel rates and τ_f in [29]. The predicted rates match the data well, with the exponentially suppressed interzone rate dominating at small frequencies and crossing over to the polynomially suppressed intrazone rate at larger frequencies, $\omega \gtrsim 6$.

Furthermore, TDPT provides more than just a FGR rate - it can also produce quantitatively accurate fidelity decay curves. Fig. 2 compares the numerically exact fidelity for an eigenstate of H_0 in the $S^z = 0$ sector with energy close to that of the scar state to the results from second-order TDPT applied to $V(t)$ for different drive frequencies (see Eq. (4)). The two compare well at all times for small frequencies, and at early times for large frequencies.

The interzone and intrazone rates also accurately describe the fidelity decay of scarred eigenstates of H_0 . Fig. 3(b) compares the decay timescale for the scar state in the $S^z = 0$ sector to an eigenstate with a similar energy. The scar is noticeably longer-lived, especially in the large frequency regime where the scar lifetime is an order of magnitude larger than that of the non-scarred eigenstate.

We interpret this behavior in terms of the spectral functions of V and $[V, [H_0, V]]$, which set the interzone and intrazone rates respectively (Eqs. (5) and (6)). In (c) and (d), we plot these spectral functions evaluated at zero frequency and see that the scar state is an outlier relative to other states in the same symmetry sector - the smaller values of the spectral function lead to smaller decay rates. Note that $\mathcal{A}_\psi^V(0)$ does not enter the interzone rate directly except for setting an overall scale for the rapidly decaying $\mathcal{A}_\psi^V(\pm\omega)$, while $\mathcal{A}_\psi^{[V, [H_0, V]]}(0)$ enters the

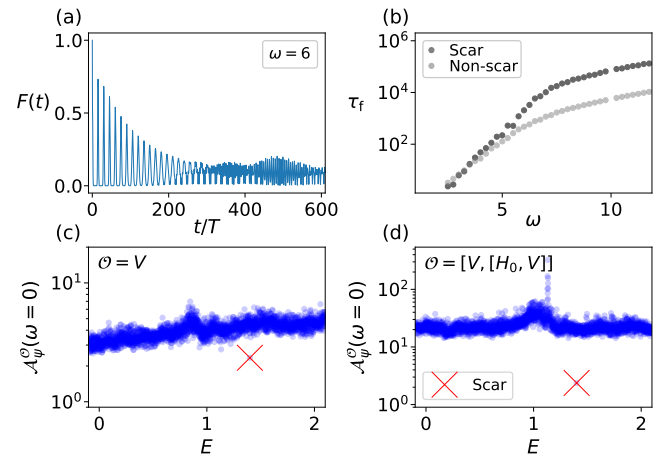


FIG. 3. (a) Fidelity dynamics of the scarred product state $\bigotimes_{i=1}^L \frac{|+\rangle_i + (-1)^i |-\rangle_i}{\sqrt{2}}$ for time evolution with $H(t) + hS^z$ with $L = 14$ and $h = .2$. The fidelity exhibits long-lived oscillations. The remaining panels consider the scar state in the $S^z = 0$ sector for comparison to other eigenstates in the same sector of H_0 . Panel (b) shows that the lifetime of the scarred eigenstate far exceeds that of the eigenstate next to the scar state in energy at large frequencies. Panels (c) and (d) show the spectral functions $f(0)$ of eigenstates of H_0 as a function of energy for V and $[V, [H_0, V]]$ respectively. The scar state is an outlier with smaller values; the smaller $[V, [H_0, V]]$ spectral function in particular is responsible for the large- ω difference between the scar and an eigenstate of similar energy in (b).

intrazone rate directly. The small value of $\mathcal{A}_\psi^{[V, [H_0, V]]}(0)$ in the scar state relative to neighboring eigenstates in energy explains the order-of-magnitude larger lifetime of the scarred state at large frequencies.

The long lifetimes of scars at large frequencies are reflected in the dynamics of product states formed from superpositions of scar states. The product state $\bigotimes_{i=1}^L \frac{|+\rangle_i + (-1)^i |-\rangle_i}{\sqrt{2}}$, which is a superposition of scar states from different S^z sectors, shows perfect oscillations of period $\frac{\pi}{h}$ under the dynamics of $H_0 + hS^z$. As seen in Fig. 3(a), under the full dynamics of $H(t) + hS^z$, there are still long-lived oscillations for large driving frequencies despite the scar-breaking drive in $H(t)$. Note that the product state decays faster than the scar state in the $S^z = 0$ sector in Fig. 3(b). The product state is a superposition of the scarred states in even S^z sectors; as the size of the relevant matrix elements of V and $[V, [H_0, V]]$ differ from sector to sector, we do not expect the same decay rate as in (b).

Discussion- We have analytically and numerically shown that the eigenstates of H_0 survive for long times under high frequency driving. In particular, the fidelity decay timescale τ_f grows exponentially with drive frequency in a wide frequency range before crossing over to a quartic dependence. The two regimes correspond to the respective dominance of interzone and intrazone channels for decay, with analytical expressions for the

decay rates given for a sinusoidal drive in Eqs. (5) and (6) and for more general drives in the Supplementary Material [29].

Our results hold for all eigenstates of H_0 ; for scar states with non-thermal local density matrices, local density matrices do not relax for long times. Thus classic signatures of quantum scarring, such as persistent oscillations in local densities, are robust to generic high frequency driving, which is promising for Floquet engineering approaches for generating scarred Hamiltonians. An interesting direction for future work is to determine the generality of Fig. 3(b), that is, whether scarred states generically live longer.

Finally, there is a close relationship between prethermalization at rapid drive frequencies ω and $U(1)$ prethermalization in the presence of a large magnetic field hS^z via analogy between the Floquet zones and magnetization sectors. In the case of $U(1)$ prethermalization with a Hamiltonian $H = H_0 + hS^z + \lambda V$ with H_0 conserving $U(1)$ and V breaking $U(1)$, a perturbation like $V = S^x$ induces “interzone” and “intrazone” processes between and within magnetization sectors of H_0 in time-dependent perturbation theory, with similar exponential and polynomial suppression in h . However, there is an important difference: in the driven case, the matrix elements coupling a Floquet zone to its neighbor at a harmonic ω above and to its neighbor at a harmonic ω below are guaranteed to be the same. More conditions are needed to guarantee this matching of matrix elements in the $U(1)$ case. For example, this is guaranteed in the $U(1)$ case for an initial state in the $S^z = 0$ sector of H_0 in the presence of a spin-flip $S^z \leftrightarrow -S^z$ symmetry generated by $U = e^{i\pi S^x}$; specifically, it requires $U^\dagger H_0 U = H_0$ and $U^\dagger V U \propto V$. When these conditions are met, the

magnetic intrazone processes undergo a similar cancellation to the driven intrazone processes with an asymptotic timescale scaling as h^4 . More generically, when these conditions are not met, the intrazone processes lead to a faster decay timescale scaling as h^2 . However, in either case, these asymptotic regimes can first be preceded by an interzone timescale growing exponentially in h . This connection to $U(1)$ prethermalization is especially notable because it has been shown that a large number of scarred models can be derived starting from models with an underlying Lie algebra, with scars living in different $U(1)$ sectors [38–40]. The energies of the scar states can be split to obtain “towers” of scar states by adding a $U(1)$ field. The discussion above means that a large magnitude for this $U(1)$ field can then be used to endow scars with a prethermal robustness to perturbations that break the $U(1)$ symmetry.

Acknowledgements— We are grateful to Sarang Gopalakrishnan, Wen Wei Ho, David Huse, Tomotaka Kuwahara, David Long, Alan Morningstar, Anatoli Polkovnikov and Marcos Rigol for useful discussions. This work was supported by the US Department of Energy, Office of Science, Basic Energy Sciences, under Early Career Award Nos. DE-SC0021111 (N.O. and V.K.), and the NSF under NSF DMR-1752759 (A.C.) and NSF DMR-1928166 (F. B.). V.K. also acknowledges support from the Alfred P. Sloan Foundation through a Sloan Research Fellowship and the Packard Foundation through a Packard Fellowship in Science and Engineering. Numerical simulations were performed on Stanford Research Computing Center’s Sherlock cluster. We acknowledge the hospitality of the Kavli Institute for Theoretical Physics at the University of California, Santa Barbara (supported by NSF Grant PHY-1748958).

[1] N. Goldman and J. Dalibard, “Periodically driven quantum systems: Effective hamiltonians and engineered gauge fields,” *Phys. Rev. X* **4**, 031027 (2014).

[2] Marin Bukov, Luca D’Alessio, and Anatoli Polkovnikov, “Universal high-frequency behavior of periodically driven systems: from dynamical stabilization to floquet engineering,” *Advances in Physics* **64**, 139–226 (2015).

[3] André Eckardt, “Colloquium: Atomic quantum gases in periodically driven optical lattices,” *Rev. Mod. Phys.* **89**, 011004 (2017).

[4] Takashi Oka and Sota Kitamura, “Floquet engineering of quantum materials,” *Annual Review of Condensed Matter Physics* **10**, 387–408 (2019).

[5] Mark S. Rudner and Netanel H. Lindner, “Band structure engineering and non-equilibrium dynamics in floquet topological insulators,” *Nature Reviews Physics* **2**, 229–244 (2020).

[6] Fenner Harper, Rahul Roy, Mark S. Rudner, and S.L. Sondhi, “Topology and broken symmetry in floquet systems,” *Annual Review of Condensed Matter Physics* **11**, 345–368 (2020).

[7] Takuya Kitagawa, Erez Berg, Mark Rudner, and Eugene Demler, “Topological characterization of periodically driven quantum systems,” *Phys. Rev. B* **82**, 235114 (2010).

[8] Netanel H Lindner, Gil Refael, and Victor Galitski, “Floquet topological insulator in semiconductor quantum wells,” *Nature Physics* **7**, 490–495 (2011).

[9] V. Khemani, A. Lazarides, R. Moessner, and S. L. Sondhi, “Phase structure of driven quantum systems,” *Phys. Rev. Lett.* **116**, 250401 (2016).

[10] Xiao Mi, Matteo Ippoliti, Chris Quintana, Ami Greene, Zijun Chen, Jonathan Gross, Frank Arute, Kunal Arya, Juan Atalaya, Ryan Babbush, *et al.*, “Time-crystalline eigenstate order on a quantum processor,” *Nature* **601**, 531–536 (2022).

[11] Luca D’Alessio and Marcos Rigol, “Long-time behavior of isolated periodically driven interacting lattice systems,” *Phys. Rev. X* **4**, 041048 (2014).

[12] Achilleas Lazarides, Arnab Das, and Roderich Moessner, “Equilibrium states of generic quantum systems subject to periodic driving,” *Phys. Rev. E* **90**, 012110 (2014).

[13] Wen Wei Ho, Takashi Mori, Dmitry A. Abanin, and Emanuele G. Dalla Torre, “Quantum and classical flo-

quet prethermalization,” *Annals of Physics* **454**, 169297 (2023).

[14] Dmitry A. Abanin, Wojciech De Roeck, and François Huveneers, “Exponentially slow heating in periodically driven many-body systems,” *Phys. Rev. Lett.* **115**, 256803 (2015).

[15] Takashi Mori, Tomotaka Kuwahara, and Keiji Saito, “Rigorous bound on energy absorption and generic relaxation in periodically driven quantum systems,” *Phys. Rev. Lett.* **116**, 120401 (2016).

[16] Tomotaka Kuwahara, Takashi Mori, and Keiji Saito, “Floquet-magnus theory and generic transient dynamics in periodically driven many-body quantum systems,” *Annals of Physics* **367**, 96–124 (2016).

[17] Marin Bukov, Markus Heyl, David A. Huse, and Anatoli Polkovnikov, “Heating and many-body resonances in a periodically driven two-band system,” *Phys. Rev. B* **93**, 155132 (2016).

[18] Krishnanand Mallayya and Marcos Rigol, “Heating rates in periodically driven strongly interacting quantum many-body systems,” *Physical Review Letters* **123** (2019), 10.1103/physrevlett.123.240603.

[19] David J. Luitz, Roderich Moessner, S. L. Sondhi, and Vedika Khemani, “Prethermalization without temperature,” *Phys. Rev. X* **10**, 021046 (2020).

[20] Dominic V. Else, Bela Bauer, and Chetan Nayak, “Prethermal phases of matter protected by time-translation symmetry,” *Phys. Rev. X* **7**, 011026 (2017).

[21] Antonio Rubio-Abadal, Matteo Ippoliti, Simon Hollerith, David Wei, Jun Rui, S. L. Sondhi, Vedika Khemani, Christian Gross, and Immanuel Bloch, “Floquet prethermalization in a bose-hubbard system,” *Phys. Rev. X* **10**, 021044 (2020).

[22] Alan Morningstar, Markus Hauru, Jackson Beall, Martin Ganahl, Adam G.M. Lewis, Vedika Khemani, and Guifre Vidal, “Simulation of quantum many-body dynamics with tensor processing units: Floquet prethermalization,” *PRX Quantum* **3**, 020331 (2022).

[23] Alan Morningstar, David A. Huse, and Vedika Khemani, “Universality classes of thermalization for mesoscopic floquet systems,” (2022).

[24] M. Aidelsburger, M. Atala, M. Lohse, J. T. Barreiro, B. Paredes, and I. Bloch, “Realization of the hofstadter hamiltonian with ultracold atoms in optical lattices,” *Phys. Rev. Lett.* **111**, 185301 (2013).

[25] Gregor Jotzu, Michael Messer, Rémi Desbuquois, Martin Lebrat, Thomas Uehlinger, Daniel Greif, and Tilman Esslinger, “Experimental realization of the topological haldane model with ultracold fermions,” *Nature* **515**, 237–240 (2014).

[26] Nick Fläschner, BS Rem, M Tarnowski, D Vogel, D-S Lühmann, K Sengstock, and Christof Weitenberg, “Experimental reconstruction of the berry curvature in a floquet bloch band,” *Science* **352**, 1091–1094 (2016).

[27] N. R. Cooper, J. Dalibard, and I. B. Spielman, “Topological bands for ultracold atoms,” *Rev. Mod. Phys.* **91**, 015005 (2019).

[28] D. Bluvstein, A. Omran, H. Levine, A. Keesling, G. Semeghini, S. Ebadi, T. T. Wang, A. A. Michailidis, N. Maskara, W. W. Ho, S. Choi, M. Serbyn, M. Greiner, V. Vuletić, and M. D. Lukin, “Controlling quantum many-body dynamics in driven Rydberg atom arrays,” *Science* **371**, 1355–1359 (2021).

[29] See Supplementary Material for details on time-dependent perturbation theory and the Floquet-Magnus expansion.

[30] Thomas Gorin, Tomaž Prosen, Thomas H. Seligman, and Marko Žnidarič, “Dynamics of loschmidt echoes and fidelity decay,” *Physics Reports* **435**, 33–156 (2006).

[31] David A. Zarate-Herrada, Lea F. Santos, and E. Jonathan Torres-Herrera, “Generalized survival probability,” *Entropy* **25** (2023), 10.3390/e25020205.

[32] Naoto Shiraishi and Takashi Mori, “Systematic Construction of Counterexamples to the Eigenstate Thermalization Hypothesis,” *Phys. Rev. Lett.* **119**, 030601 (2017).

[33] Hannes Bernien, Sylvain Schwartz, Alexander Keesling, Harry Levine, Ahmed Omran, Hannes Pichler, Soonwon Choi, Alexander S. Zibrov, Manuel Endres, Markus Greiner, Vladan Vuletić, and Mikhail D. Lukin, “Probing many-body dynamics on a 51-atom quantum simulator,” *Nature* **551**, 579–584 (2017).

[34] Maksym Serbyn, Dmitry A. Abanin, and Zlatko Papić, “Quantum many-body scars and weak breaking of ergodicity,” *Nature Physics* **17**, 675–685 (2021).

[35] Sanjay Moudgalya, B Andrei Bernevig, and Nicolas Regnault, “Quantum many-body scars and hilbert space fragmentation: a review of exact results,” *Reports on Progress in Physics* **85**, 086501 (2022).

[36] Anushya Chandran, Thomas Iadecola, Vedika Khemani, and Roderich Moessner, “Quantum many-body scars: A quasiparticle perspective,” *Annual Review of Condensed Matter Physics* **14**, 443–469 (2023).

[37] Michael Schechter and Thomas Iadecola, “Weak Ergodicity Breaking and Quantum Many-Body Scars in Spin-1 X Y Magnets,” *Phys. Rev. Lett.* **123**, 147201 (2019).

[38] Daniel K. Mark, Cheng-Ju Lin, and Olexei I. Motrunich, “Unified structure for exact towers of scar states in the Affleck-Kennedy-Lieb-Tasaki and other models,” *Phys. Rev. B* **101**, 195131 (2020).

[39] Nicholas O’Dea, Fiona Burnell, Anushya Chandran, and Vedika Khemani, “From tunnels to towers: Quantum scars from Lie algebras and q -deformed Lie algebras,” *Phys. Rev. Research* **2**, 043305 (2020).

[40] K. Pakrouski, P.N. Pallegar, F.K. Popov, and I.R. Klebanov, “Many-Body Scars as a Group Invariant Sector of Hilbert Space,” *Phys. Rev. Lett.* **125**, 230602 (2020).

Supplemental Material for: Prethermal stability of eigenstates under high frequency Floquet driving

Nicholas O'Dea,¹ Fiona Burnell,² Anushya Chandran,³ and Vedika Khemani¹

¹*Department of Physics, Stanford University, Stanford, CA 94305, USA*

²*Department of Physics, University of Minnesota Twin Cities, MN 55455, USA*

³*Department of Physics, Boston University, MA 02215, USA*

In this supplemental material, we share some additional numerics exploring heating and reduced density matrices, and we explain the details of how we extracted timescales from fidelity curves. We then give a detailed discussion of time-dependent perturbation theory for the log of the fidelity, with explicit expressions for interzone and intrazone rates given in Eqs. S43 and S48 and specifically for the box drive in Eqs. S45 and S50.

I. ADDITIONAL DETAILS ON NUMERICS

A. Heating versus fidelity

In this section, we clarify how heating and fidelity curves are influenced by the initial state. In particular, we compare an eigenstate of H_0 to a product state that is not an eigenstate of H_0 but has the same energy density.

Proofs of prethermalization show that heating is slow regardless of the initial state: this is clear in Fig. S1 c) and d), where both of these initial states show heating that is exponentially slow in frequency.

However, the results of our paper on long-lived fidelity only apply to all eigenstates of H_0 . In particular, despite slow heating, the product state fidelity in Fig. S1b) rapidly decays in an $O(1)$ time. On the other hand, the eigenstate of H_0 indeed shows a long-lived fidelity in Fig. S1a).

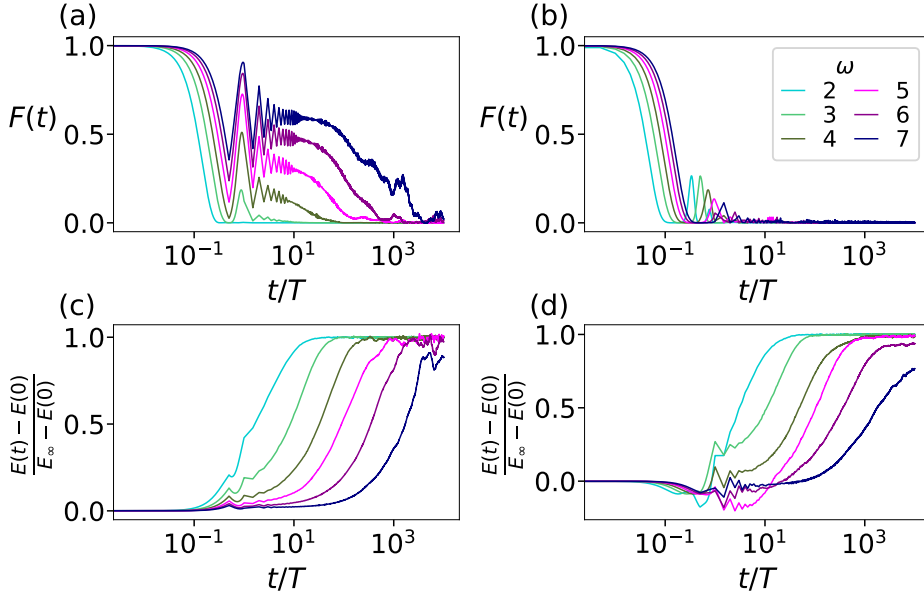


FIG. S1. Fidelity against time for (a) an eigenstate of H_0 and (b) a product state at the same energy density of .56. c) and d) show heating curves for the same eigenstate of H_0 and product state respectively. $L = 14$, and the eigenstate is an energy density .56 eigenstate taken from the momentum $k = 0$, magnetization $S^z = 0$, inversion-symmetric, spin-flip-symmetric sector of H_0 . The product state is at the same energy density and is proportional to $\bigotimes_{j=1}^L (\cos(\theta)|+\rangle_j + \sqrt{2}\sin(\theta)|0\rangle_j + \cos(\theta)|-\rangle_j)$ for $\theta = 3\pi/8$.

B. Timescale extraction

In the main text, we extract timescales from fidelity curves against time, $F(t)$, and compare those timescales to Fermi's Golden Rule (FGR) predictions. In this appendix, we make our fitting procedure for extracting timescales from $F(t)$ explicit.

We choose to fit our data to an ansatz of $F(t) = ce^{-t/\tau_f}$ for a limited range of times. Using a limited window to fit was motivated by the fact that FGR does not hold at early times and because our data may be susceptible to finite-size effects at very long times. We indeed begin to see oscillations in the fidelity at late times and large frequencies in Fig. S2a). The fitting windows for each $F(t)$ curve are explicitly shown in Fig. S2a), where we linearly interpolated between a window of $[1, 3]$ and a window of $[20, 200]$ for frequencies between $\omega = 2.5$ and 14.75 .

C. Numerically estimating the FGR predictions

In the main text, we compare extracted timescales (see above subsection) to predictions from Fermi's Golden Rule. In this subsection, we explain how we numerically calculate these analytical FGR predictions.

For the box drive considered in the main text, the FGR interzone and intrazone predictions for the fidelity decay rates of an eigenstate $|i\rangle$ of H_0 (derived in Section 2 of the supplementary material in Eqs. S45 and S50) are

$$R_i^{\text{inter}} = \frac{8\lambda^2}{\pi} \sum_{n=0}^{\infty} \frac{\mathcal{A}_i^V((2n+1)\omega) + \mathcal{A}_i^V(-(2n+1)\omega)}{(2n+1)^2} \quad (\text{S1})$$

$$R_i^{\text{intra}} \approx \frac{\pi^5 \lambda^4}{288\omega^4} \mathcal{A}_i^{[V, [H_0, V]]}(0) \quad (\text{S2})$$

where the spectral functions are defined as

$$\mathcal{A}_i^O(\omega) = \sum_j |O_{ij}|^2 \delta((E_i - E_j) - \omega) \quad (\text{S3})$$

in the eigenbasis of H_0 .

We compute the spectral functions by diagonalizing H_0 and replacing the delta function $\delta((E_i - E_j) - \omega)$ with a normalized indicator function $\frac{1}{W} \mathbb{1}_{|(E_i - E_j) - \omega| \leq W/2}$ for a small energy window W . We also truncate the sum over harmonics in Eq. S1, which is valid because the spectral functions are rapidly decaying as a function of their arguments. In the main text, we use $W = .2$ and truncate the sum in Eq. S1 to include the first six terms.

D. Local reduced density matrices

In the main text, the primary quantity we probe is the many-body fidelity $F(t)$. As noted above, the fidelity decays with a rate that is extensive in system size. Here we consider the reduced density matrix on an $O(1)$ number of sites, $\rho(t)$, which should be asymptotically insensitive to system size at finite times.

In particular, in Fig. S2a), we calculate the change in the two-site reduced density matrix $\rho(t)$ relative to its initial condition $\rho(t=0)$ for the scar state in the $S^z = 0$ sector of H_0 . Specifically, we compute $\|\rho(t) - \rho(0)\|$ where $\|A\| = \text{Tr}(\sqrt{A^\dagger A})$ is the trace-norm. This is a nice norm because it bounds the change in observables:

$$\text{Tr}[(\rho(t) - \rho(0))O] \leq \|\rho(t) - \rho(0)\| \sigma_{\max}(O)$$

where $\sigma_{\max}(O)$ is the largest singular value of the operator O . We see that the curves are not changing much as a function of system size, showing that our time-dependent results have largely converged at these times and frequencies.

Note that for non-scarred eigenstates of H_0 at similar energies to that of the scar, $\rho(0)$ already looks highly mixed, and so $\rho(t)$ is largely insensitive to the drive; i.e. $\|\rho(t) - \rho(0)\|$ is close to zero at all times for such states.

II. TIME-DEPENDENT PERTURBATION THEORY

A. Dyson series for the interaction picture $U_I(t)$

We consider a Hamiltonian of the general form:

$$H(t) = H_0 + \lambda g(t)V \quad (\text{S4})$$

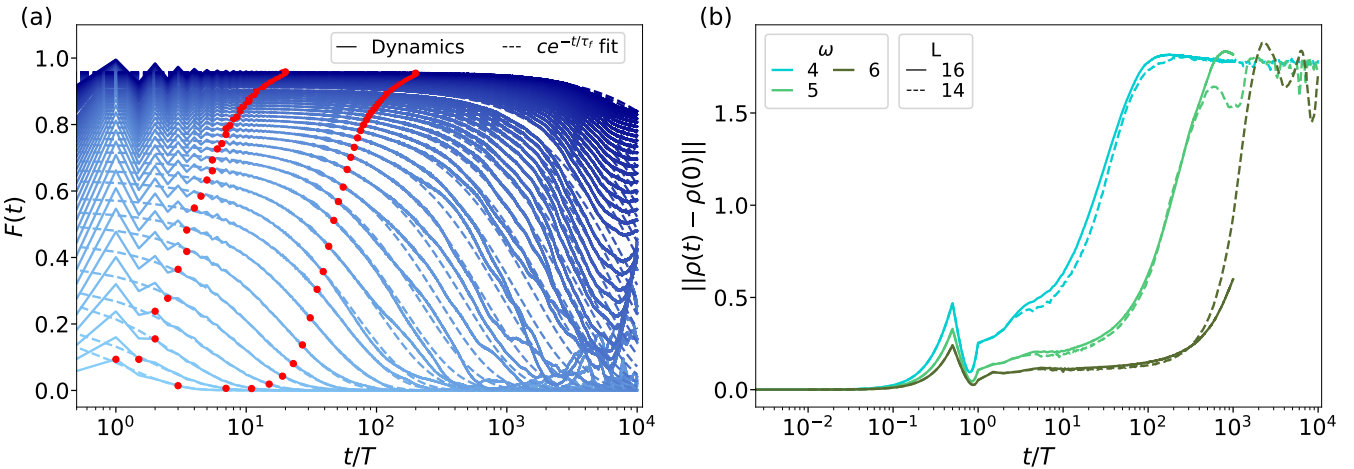


FIG. S2. a) Plotting the fidelity against time, $F(t)$, for an eigenstate of H_0 at zero energy density driven by $H(t)$ (Eq. 7), same as in Fig. 1a) in the main text. Here we show the curves for frequencies between $\omega = 2.5$ and 14.75 in steps of $.25$ from light to dark blue. Between each pair of red dots we fit a given $F(t)$ curve to the ansatz $F(t) = ce^{-t/\tau_f}$, and the resulting τ_f are used in Fig. 1b), “Dynamics”, in the main text. The dotted lines show the resulting ce^{-t/τ_f} curves. b) Trace-norm of the difference between $\rho(t)$ and $\rho(0)$ for the scar state in the $S^z = 0$ sector of H_0 for system sizes $L = 14, 16$.

The time evolution by $H(t) = H_0 + V(t)$ is generated by $U(t) = U_I(t)U_0(t)$, where $U_0 = e^{-iH_0t}$ and $U_I(t)$ is the unitary time-evolution operator in the interaction picture. $U_I(t)$ can be expanded in the Dyson series:

$$U_I(t) = \sum_{n=0}^{\infty} U^{(n)} \quad (S5)$$

$$U_{ij}^{(n)} = (-i\lambda)^n \int_0^t \int_0^{t_1} \dots \int_0^{t_{n-1}} dt_1 \dots dt_n \left(\prod_{j=1}^n f(t_j) \right) \langle i | V(t_1) \dots V(t_n) | j \rangle$$

where $U^{(0)} \equiv 1$, and $V(t) \equiv U_0^\dagger(t) V U_0(t)$.

To simplify the expression for $U_{ij}^{(n)}$, we express the periodic drive $g(t)$ as a Fourier series $g(t) = \sum_p c_p e^{ip\omega t}$, where the fundamental frequency ω defines the period of the drive. Inserting a complete set of eigenstates of H_0 between each power of V , we obtain:

$$U_{j_0 j_n}^{(n)} = (-i\lambda)^n \sum_{p_1 \dots p_n} c_{p_1} \dots c_{p_n} \sum_{j_1, j_2, \dots, j_{n-1}} V_{j_0 j_1} V_{j_1 j_2} \dots V_{j_{n-1} j_n} \int_0^t \int_0^{t_1} \dots \int_0^{t_{n-1}} dt_1 \dots dt_n \prod_{q=1}^n e^{i\Omega_q t_q} \quad (S6)$$

where

$$\Omega_l = \Delta_{j_{l-1} j_l} + p_l \omega, \quad \Delta_{ij} = \epsilon_j - \epsilon_i \quad (S7)$$

with ϵ_j the unperturbed energy of eigenstate $|j\rangle$ of H_0 .

To simplify this expression, we use the following identity:

$$\prod_{i=1}^n \left[\int_0^{t_{i-1}} dt_i \right] \prod_{k=1}^n e^{i\Omega_k t_k} = \frac{1}{i^n} \sum_{k=1}^n \frac{e^{iS_{0,k} t_0} - 1}{\prod_{m=0; m \neq k}^n S_{m,k}} \quad (S8)$$

where

$$S_{m,k} = \begin{cases} \sum_{l=m+1}^k \Omega_l & m < k \\ -S_{k,m} & m > k \end{cases} \quad (S9)$$

Inserting this in to Eq. (S6), we obtain the general expression:

$$U_{j_0 j_n}^{(n)} = (-\lambda)^n \sum_{p_1 \dots p_n} c_{p_1} \dots c_{p_n} \sum_{j_1, j_2, \dots, j_{n-1}} V_{j_0 j_1} V_{j_1 j_2} \dots V_{j_{n-1} j_n} \sum_{k=1}^n \frac{e^{iS_{0,k} t_0} - 1}{\prod_{m \neq k; m \geq 0}^n S_{m,k}} \quad (S10)$$

which holds provided that $S_{mk} \neq 0$ for any pair m, k . (We discuss the terms with $S_{mk} = 0$, known as secular terms, below).

To show that Eq. (S8) holds for general n , we proceed by induction. For $n = 1$, the identity gives:

$$\int_0^{t_0} dt_1 e^{i\Omega_1 t_1} = \frac{1}{i} \frac{e^{i\Omega_1 t_0} - 1}{\Omega_1} \quad (\text{S11})$$

where we have used $S_{01} = \Omega_1$. This is clearly true. Therefore, let us assume that the formula holds for up to $n - 1$ terms. Then, since $\Omega_1 + S_{1k} = S_{0k}$:

$$\prod_{i=1}^n \left[\int_0^{t_{i-1}} dt_i \right] \prod_{k=1}^n e^{i\Omega_k t_k} = \frac{1}{i^{n-1}} \int_0^{t_0} dt_1 \left(\sum_{k=2}^n \frac{e^{iS_{0k} t_1}}{\prod_{m \neq k; m \geq 1} S_{mk}} - e^{i\Omega_1 t_1} \sum_{k=2}^n \frac{1}{\prod_{m \neq k; m \geq 1} S_{mk}} \right) \quad (\text{S12})$$

We simplify the second term by noting that $\sum_{k=1}^n \frac{1}{\prod_{m \neq k; m \geq 1} S_{mk}} = 0$. (This follows from the fact that, for any set of numbers $\{x_j\}_{j=1}^n$, $\sum_j \prod_{k \neq j} \frac{1}{x_j - x_k} = 0$. We take $x_j = \epsilon_j + \sum_{h=j+1}^n \Omega_h$, such that $x_j - x_k = S_{jk}$.) Thus we can simplify

$$-e^{i\Omega_1 t_1} \sum_{k=2}^n \frac{1}{\prod_{m \neq k; m \geq 1} S_{mk}} = \frac{e^{iS_{01} t_1}}{\prod_{m \neq 1; m \geq 1} S_{m1}}. \quad (\text{S13})$$

This gives the desired result:

$$\prod_{i=1}^n \left[\int_0^{t_{i-1}} dt_i \right] \prod_{k=1}^n e^{i\Omega_k t_k} = \frac{1}{i^{n-1}} \int_0^{t_0} dt_1 \sum_{k=1}^n \frac{e^{iS_{0k} t_1}}{\prod_{m \neq k; m \geq 1} S_{mk}} = \frac{1}{i^n} \sum_{k=1}^n \frac{e^{iS_{0k} t_1} - 1}{\prod_{m \neq k; m \geq 0} S_{mk}}. \quad (\text{S14})$$

B. Time dependence of fidelity via cumulant expansion

Using the expression for the time evolution operator U given by time-dependent perturbation theory, we now derive a perturbative expression for $\log(F(t))$, where

$$\log(F(t)) = \log(|\langle i|U|i\rangle|^2) = 2\Re[\log((U_{ii})_{ii})] \quad (\text{S15})$$

The n^{th} order term in this series is simply the real part of the n^{th} order term in the cumulant expansion of U_{ii} . The general expressions for such cumulants can be found in [1].

A property of some of the models of interest to us is that the Hamiltonian H_0 has a $U(1)$ symmetry, such that the total spin in the z direction S^z is conserved. The perturbation $V = \sum_i S_i^x$, on the other hand, breaks this symmetry by changing the value of S^z by exactly ± 1 . It follows that for any eigenstate $|i\rangle$ of H_0 , $\langle i|V^{2n+1}|i\rangle = 0$, since the states $|i\rangle$ and $V^{2n+1}|i\rangle$ cannot have the same value of S^z . This means that there are no secular terms in $U^{(1)}$, and that $U_{ii}^{(2n+1)} = 0$. In the following discussions, we will assume the existence of such a symmetry, and drop any terms involving odd powers of V from our calculation of $\log(F(t))$. Note that this structure is *not* essential to our main results; allowing $\langle i|V^{2n+1}|i\rangle \neq 0$ will only yield subleading-in- λ corrections to the computed rates.

To fourth order, with $U_{ii}^{(2n+1)} = 0$, Eq. (S15) gives:

$$\begin{aligned} \log F(t) &= 2\Re \left(U_{ii}^{(2)} + (U_{ii}^{(4)} - \frac{1}{2}(U_{ii}^{(2)})^2) + O(\lambda^6) \right) \\ &= 2\Re \left(U_{ii}^{(2)} \right) + (2\Re \left(U_{ii}^{(4)} \right) - \Re \left(U_{ii}^{(2)} \right)^2 + \Im \left(U_{ii}^{(2)} \right)^2) + O(\lambda^6) \end{aligned} \quad (\text{S16})$$

We note that one could also consider a perturbative expansion for the fidelity itself, which takes the form:

$$\begin{aligned} F(t) &= (1 + U_{ii}^{(2)} + U_{ii}^{(4)} + \dots)(1 + U_{ii}^{(2)} + U_{ii}^{(4)} + \dots)^* \\ &= (1 + (U_{ii}^{(2)} + U_{ii}^{(2)*}) + (U_{ii}^{(4)} + U_{ii}^{(2)}U_{ii}^{(2)*} + U_{ii}^{(4)*})) + O(\lambda^6) \\ &= 1 + 2\Re(U_{ii}^{(2)}) + (2\Re(U_{ii}^{(4)}) + |U_{ii}^{(2)}|^2) + O(\lambda^6) \end{aligned} \quad (\text{S17})$$

While the two expansions will match when all orders of perturbation theory are included, this form for $F(t)$ has two disadvantages. First, at finite order in λ , it is not positive-definite, and indeed typically does fall below zero for some

times when truncated at a low order in perturbation theory. Second, a natural ansatz for the behavior of the fidelity is

$$F(t) = e^{-L^d f(\lambda, t)}, \quad (\text{S18})$$

which is expected because in a given time, there are $O(L^d)$ local changes in the initial state that can contribute to fidelity decay. If this ansatz is correct, then the truncated cumulant expansion that describes $\log(F(t))$ should be proportional to L^d order by order in λ , while in the expansion (S17), multiple powers of L^d appear at a given order of λ .

C. $\log(F)$ to fourth order in λ

Using the cumulant expansion (S16), we can calculate the fourth-order correction to the fidelity. Some care must be taken with secular terms. Most of the terms in the series can be obtained from the fourth order terms in (S10) by Taylor expanding to leading order in S_{02} and S_{04} respectively. The resulting secular terms grow linearly in time, and are purely imaginary. At fourth order, however, additional secular terms are possible, and we must also account for the possibility that $S_{13} = 0$ and $S_{02} = S_{24} = 0$. These terms are not captured by the leading order Taylor expansion, but can be calculated directly from Eq. (S6).

For convenience, we will assume that all coefficients c_{p_j} are either purely real, or purely imaginary, such that any product of an even number of these is real. In this case, we find:

$$\begin{aligned} 2\Re(U_{ii}^{(2)}) &= -4\lambda^2 \sum_j |V_{ij}|^2 \left(\sum_{p_1, p_2} c_{p_1} c_{p_2} \frac{\sin^2(S_{ij}t/2)}{S_{ij}(\Delta_{ij} - p_2\omega)} - \sum_{p_1 \neq -p_2} c_{p_1} c_{p_2} \frac{\sin^2(\omega(p_1 + p_2)t/2)}{\omega(p_1 + p_2)(\Delta_{ij} - p_2\omega)} \right) \quad (\text{S19}) \\ 2\Re(U_{ii}^{(4)}) + \Im(U_{ii}^{(2)})^2 &= 2\lambda^4 \sum_{p_1, p_2, p_3, p_4} c_{p_1} c_{p_2} c_{p_3} c_{p_4} \sum_{j, k, l} V_{ij} V_{jk} V_{kl} V_{li} \left((1 - \delta_{S_{ik}}) \left(\frac{\sin^2(S_{ik}t/2)}{S_{ik} S'_{ki} S_{jk} S_{lk}} \right) \right. \\ &\quad \left. + (1 - \delta_{p_1 + p_2 + p_3 + p_4}) \frac{\sin^2(\omega(p_1 + p_2 + p_3 + p_4)t/2)}{S'_{il} S'_{ik} S'_{ij} \omega(p_1 + p_2 + p_3 + p_4)} \right. \\ &\quad \left. + (1 - \delta_{S_{jl}}) \left(\frac{\sin^2(S_{ij}t/2)}{S_{ij} S'_{ji} S_{lj} S_{kj}} + \frac{\sin^2(S_{il}t/2)}{S_{il} S'_{li} S_{jl} S_{kl}} \right) \right) \\ &\quad + \sum_{k, l} \delta_{p_2 + p_3} |V_{kl}|^2 |V_{il}|^2 \left(\frac{\sin^2(S_{il}t/2)(2S_{kl} + S_{il})}{S_{kl}^2 S_{il}^3} - \frac{2t \sin(tS_{il})}{S_{kl} S_{il} S'_{il}} \right) \quad (\text{S20}) \\ &\quad + \left(\sum_j |V_{ij}|^2 \sum_{p_1, p_2} c_{p_1} c_{p_2} \frac{\sin(S_{ij}t)}{S_{ij}(\Delta_{ij} - p_2\omega)} - \sum_{p_1 \neq -p_2} c_{p_1} c_{p_2} \frac{\sin \omega(p_1 + p_2)t}{\omega(p_1 + p_2)(\Delta_{ij} - \omega p_2)} \right)^2 \\ &\quad - 2 \sum_{l, p_3 = -p_4} c_{p_3} c_{p_4} \frac{t}{\Delta_{il} - \omega p_4} \sum_j |V_{ij}|^2 \left(\sum_{p_1, p_2} c_{p_1} c_{p_2} \frac{\sin(S_{ij}t)}{S_{ij}(\Delta_{ij} - \omega p_2)} \right. \\ &\quad \left. - \sum_{p_1 \neq -p_2} c_{p_1} c_{p_2} \frac{\sin \omega(p_1 + p_2)t}{\omega(p_1 + p_2)(\Delta_{ij} - \omega p_2)} \right) \end{aligned}$$

where, from Eq. (S9)

$$\begin{aligned} S_{ij} &= \Delta_{ij} + \omega p_1, \quad S_{ik} = \Delta_{ik} + \omega p_1 + \omega p_2, \quad S_{il} = \Delta_{il} + \omega p_1 + \omega p_2 + \omega p_3, \quad S_{jk} = \Delta_{jk} + \omega p_2, \quad S_{jl} = \Delta_{jl} + \omega p_2 + \omega p_3 \\ S_{kl} &= \Delta_{kl} + \omega p_3, \quad S'_{ij} = -\Delta_{ij} + \omega p_2 + \omega p_3 + \omega p_4, \quad S'_{ik} = -\Delta_{ik} + \omega p_3 + \omega p_4, \quad S'_{il} = -\Delta_{il} + \omega p_4 \end{aligned} \quad (\text{S21})$$

and as usual, $S_{ba} = -S_{ab}$, and similarly for S' . We note that though both $2\Re(U_{ii}^{(4)})$ and $\Im(U_{ii}^{(2)})^2$ have secular terms that grow with t^2 , these cancel. Of the remaining secular terms, which are linear in t , two are multiplied by a sum of incoherent sinusoids, and thus are not expected to diverge at long times as these incoherent sums fall off faster than $1/t$ for large t . When S_{ij} is very small, they can contribute to the late-time fidelity decay, which we discuss in the next subsection; however the corresponding matrix elements are always exponentially suppressed in ω/J , and do not significantly impact the fourth-order fidelity decay.

The final contribution, of the form

$$2t \sum_j |V_{ij}|^2 \sum_{l,p_3} c_{p_4} c_{-p_4} \frac{1}{(\Delta_{il} - \omega p_4)} \sum_{p_1 \neq -p_2} c_{p_1} c_{p_2} \frac{\sin \omega(p_1 + p_2)t}{\omega(p_1 + p_2)(\Delta_{ij} - \omega p_2)} \quad (\text{S22})$$

vanishes at integer multiples of the drive period.

D. Time scales in the perturbative expansion

We now turn to the time dependence of $\log(F)$, focusing on those terms that contribute significantly to fidelity decay at long times $t \gg \omega$. We will show that these terms come in two types. At second (and leading) order in λ , the contribution to the long-time fidelity decay comes only from inter-zone terms with exponentially suppressed matrix elements; these are the terms that contribute to heating. At fourth order in λ , there are inter-zone (heating) contributions, but also intra-zone processes, which do not contribute to heating but do contribute to fidelity decay. In the next section, we will give explicit expressions for the contributions that both the second-order inter-zone and fourth order intra-zone terms make to the long-time fidelity decay rate.

With the exception of the secular terms in the last line of Eq. (S20), which do not contribute to the long-time fidelity decay at $t = nT$, where T is the drive period, we now show that each term in the sums (S19-S20) will “freeze out”, in the sense that it no longer contributes to fidelity decay, after some time.

For each term in the sums, we can identify two distinct regimes. The short-time regime describes times for which $S_{abt} \ll 1$. In this limit, we may Taylor expand the numerator to obtain:

$$\frac{\sin(S_{abt})}{S_{ab}} \approx t, \quad \frac{\sin^2(S_{abt}/2)}{S_{ab}} \approx S_{ab}t^2/4 \quad (\text{S23})$$

When $S_{abt} \sim 1$, this expansion breaks down, and we instead use the bounds:

$$\sin^2(S_{abt}/2) \leq 1, \quad |\sin(S_{abt})| \leq 1 \quad (\text{S24})$$

to upper-bound the contribution of each term to the log fidelity by a constant. (The exception to this is the secular terms involving sums of products of $t \sin S_{abt}$, for which this upper bound would yield a divergent result at large times, whereas the full sum is expected to be much smaller.) This bound is attained for $t = \pi/S_{ab}$ (or $t = \pi/(2S_{ab})$, in the second case), after which the term in question has frozen out, in the sense that it ceases to contribute to the fidelity decay.

It is worth emphasizing that the overall growth of $|U_{ij}^{(n)}|$ can be much slower than these low-order expansions of individual terms suggest, as the leading-order contributions can cancel between different terms in the sum. Such cancellations occur, for example, at very short times, when $\Omega_q t \ll 1$ for all q . In this case the integrand in Eq. (S6) is approximately constant, and $U_{ii}^{(n)} \sim \frac{(-i)^n}{n!} t^n (V^n)_{ii}$. In expressions of the form (S10), this results from the fact that when all complex exponentials are Taylor expanded, the coefficients of the first $n-1$ powers of t vanish, leaving a leading-order dependence of t^n .

To understand the fidelity decay at time t , we ignore those terms that have frozen out at shorter times, and consider a restricted sum over the remaining terms. Up to fourth order, the long-time contributions at order $2n$ come from $\Re U^{(2n)}$, and are described by a restricted sum of the form (see Eq. (S10)):

$$\frac{t^2}{4} \sum_{p_1, p_2, \dots, p_{2n}} \delta(\sum_{i=1}^n p_i) c_{p_1} c_{p_2} \dots c_{p_n} \sum_{k=1}^{2n} \left(\sum_{j_1, j_2, \dots, j_{2n-1} | S_{j_0 j_k}(p) < 2/t} V_{j_0 j_1} V_{j_1 j_2} \dots V_{j_{2n-1} j_0} \frac{S_{j_0 j_k}^2}{\prod_{m \neq k; m \geq 0} S_{j_m j_k}} \right) \quad (\text{S25})$$

Evidently, for t large compared to the drive period, we count only terms where $S_{j_0 j_k} = \Delta_{j_0 j_k}$. The number of states in the restricted sum is therefore given by

$$N(t) = \int_{\epsilon_{j_0} - \frac{1}{t}}^{\epsilon_{j_0} + \frac{1}{t}} \rho(E) dE \sim \frac{2}{t} \rho_0 \quad (\text{S26})$$

where in the final equality, we have assumed that the density of states is approximately constant, $\rho(E) \approx \rho_0$. In other words, we obtain approximately $2/(t\mathcal{J})$ of the total number of states in the sum, where \mathcal{J} is the band-width of H_0 . At long times, we can roughly approximate the restricted sum to be $2/(t\mathcal{J})$ of the unrestricted sum, giving:

$$\frac{t}{2\mathcal{J}} \sum_{p_1, p_2, \dots, p_{2n}} \delta(\sum_{i=1}^n p_i) c_{p_1} c_{p_2} \dots c_{p_n} \sum_{k=1}^{2n} \left(\sum_{j_1, j_2, \dots, j_{2n-1}} V_{j_0 j_1} V_{j_1 j_2} \dots V_{j_{2n-1} j_0} \frac{S_{j_0 j_k}^2}{\prod_{m \neq k; m \geq 0} S_{j_m j_k}} \right) \quad (\text{S27})$$

Since the term in the sum is time-independent, we therefore conclude that the log fidelity decay is approximately linear in time.

In addition to terms of the form (S25), there are contributions from cross-terms in Eqs. (S19 - S20), for which $S_{j_0 j_k}^2$ in the above expression is replaced by $S_{j_0 j_k} S_{j_0 j_l}$, and can appear with a different product of matrix elements. These also lead to a fidelity decay that is at most linear in t , albeit with a different expression for the slope. At fourth order, however, these all involve at least one high-frequency term, and thus do not contribute to the linear fidelity decay in the long-time limit.

We now discuss the slope associated with Eq. (S25), to fourth order in perturbation theory. At second order, the fidelity decay (S16) is described by $2\Re(U_{ii}^{(2)})$, given in Eq. (S19). This contains two types of terms. First, for every choice of intermediate state j , the sum contains a term proportional to $\sin^2(\omega(p_1 + p_2)t/2)$. All of these terms freeze out in the sense of having attained their maximum impact on fidelity decay at a time-scale $t \lesssim \pi/(2\omega)$. However, because there are a large number of them, all of which are coherent, at time-scales beyond this, the fidelity shows evidence of oscillations at the frequency ω . (Note that the plots shown in the main text are stroboscopic after the first period, and these oscillations are not visible).

Second, there are terms proportional to $\sin^2(S_{ij}t/2)$, with $S_{ij} = \Delta_{ij} + n\omega$, $n \in \mathbb{Z}$. As described above, a useful upper bound for each of these terms is obtained by replacing

$$\sin^2(S_{ij}t/2) \lesssim \begin{cases} (S_{ij}t)^2 & t < \frac{\pi}{S_{ij}} \\ 1 & \text{otherwise} \end{cases} \quad (\text{S28})$$

so that for $t > \frac{\pi}{S_{ij}}$, the appropriate upper bound is constant in time, and the term has frozen out. If $|\Delta_{ij}| < J$, the corresponding matrix elements are not suppressed in ω , but for $\omega \gg J$ these terms freeze out at times $t \sim 1/\omega$, and contribute to the fidelity decay only during the first few drive periods. Such terms are a dominant source of the rapid fidelity decay at early times observed in the main text. The remaining terms at second order have $\Delta_{ij} + n\omega \ll \omega$. These terms have matrix elements that are exponentially suppressed in ω/J , and make a contribution to the fidelity decay that is linear in time, but with a slope that decreases as $e^{-\omega/J}$. Thus at quadratic order, the fidelity decay at times large compared to the drive period is expected to scale as:

$$\delta \log(F(t)) \sim -L^d t \lambda^2 e^{-\omega/J} \quad (\text{S29})$$

The quartic order contribution to fidelity decay is given by $2\Re U_{ii}^{(4)} + (\Im U_{ii}^{(2)})^2 - (\Re U_{ii}^{(2)})^2$. The contributions from $(\Re U_{ii}^{(2)})^2$ either freeze out on the scale of a single drive period, or appear with matrix elements that are exponentially suppressed in ω/J . The remaining fourth-order contribution is given in Eq. (S20), and contains both terms that freeze out on the scale of a single drive period (including a contribution from coherent oscillations at frequencies $n\omega$), and terms that contribute to the long-time fidelity decay which are multiplied by matrix elements suppressed by $e^{-\omega/J}$. However, we also find a third type of term not present at second order. Taking $p_1 + p_2 = 0$, the first line of Eq. (S20) gives a contribution of the form:

$$-4 \sum_{p_1, p_3, p_4} c_{p_1} c_{-p_1} c_{p_3} c_{p_4} \sum_{j, k, l} V_{ij} V_{jk} V_{kl} V_{li} \left(\frac{\sin^2(t\Delta_{ik}/2)}{\Delta_{ik}(\Delta_{jk} - \omega p_1)(\Delta_{kl} + \omega p_3)(-\Delta_{ik} + \omega(p_3 + p_4))} \right). \quad (\text{S30})$$

For $\Delta_{ik} \lesssim J$ the corresponding matrix elements are not exponentially suppressed; thus we expect that these terms dominate the fidelity decay at times large compared to the drive period.

Thus, at long times, the dominant quartic-order contribution to the fidelity decay is described by the sum:

$$4\lambda^4 \sum_{j, k, l} V_{ij} V_{jk} V_{kl} V_{li} \frac{\sin^2(t\Delta_{ik}/2)}{\Delta_{ik}} \left[\sum_{p_1, p_3} \frac{1}{\Delta_{ik}} \frac{c_{p_1} c_{-p_1} c_{p_3} c_{-p_3}}{(\Delta_{jk} - \omega p_1)(\Delta_{kl} + \omega p_3)} \right. \\ \left. - \sum_{p_1, p_3, p_4 \neq -p_3} \frac{c_{p_1} c_{-p_1} c_{p_3} c_{p_4}}{(\Delta_{jk} - \omega p_1)(\Delta_{kl} + \omega p_3)(-\Delta_{ik} + \omega p_3 + \omega p_4)} \right] \quad (\text{S31})$$

where c_{-p_j} is the coefficient associated with $-p_j$. The sum over frequencies in the first line gives:

$$\sum_{p_1, p_3} \frac{c_{p_1} c_{-p_1} c_{p_3} c_{-p_3}}{(\Delta_{jk} - \omega p_1)(\Delta_{kl} + \omega p_3)} = \left(\sum_{p_1 > 0} \frac{c_{p_1} c_{-p_1}}{(\Delta_{jk} - \omega p_1)} + \frac{c_{p_1} c_{-p_1}}{(\Delta_{jk} + \omega p_1)} \right) \left(\sum_{p_3 > 0} \frac{c_{p_3} c_{-p_3}}{(\Delta_{kl} + \omega p_3)} + \frac{c_{p_3} c_{-p_3}}{(\Delta_{kl} - \omega p_3)} \right) \\ = \sum_{p_1 > 0, p_3 > 0} \frac{4c_{p_1} c_{-p_1} c_{p_3} c_{-p_3} \Delta_{jk} \Delta_{kl}}{(\Delta_{jk}^2 - (\omega p_1)^2)(\Delta_{kl}^2 - (\omega p_3)^2)} \quad (\text{S32})$$

If none of the matrix elements are exponentially suppressed, all energy differences must be small compared to ω , and this term is of order $1/\omega^4$, rather than $1/\omega^2\Delta_{ik}^2$ as one might naively have guessed. Similarly, summing over frequencies in the second line yields:

$$\sum_{p_1, p_3, p_4 \neq -p_3} \frac{c_{p_1} c_{-p_1} c_{p_3} c_{p_4}}{(\Delta_{jk} - \omega p_1)(\Delta_{kl} + \omega p_3)(-\Delta_{ik} + \omega(p_3 + p_4))} = \sum_{p_1 > 0} \frac{2c_{p_1} c_{-p_1} \Delta_{jk}}{(\Delta_{jk}^2 - (\omega p_1)^2)} \sum_{p_3, p_4 \neq -p_3} \left(\frac{c_{p_3} c_{p_4}}{(\Delta_{kl} + \omega p_3)(-\Delta_{ik} + \omega(p_3 + p_4))} \right) \quad (\text{S33})$$

Again, when the matrix elements are not suppressed, this denominator is of order ω^4 .

Thus, at large ω/J , the long-time fidelity decay is dominated by terms in the first line Eq. (S20), which arise at fourth order in perturbation theory. Their contribution to the fidelity decay is of the form $\delta \log(F(t)) \sim -tL^d \lambda^4/\omega^4$. These terms do not contribute to heating, as they are associated with processes that bring the system back to the original energy zone. As we discuss in Sec. III D, this scaling agrees with predictions of the Floquet Magnus expansion.

III. THREE FGR RATES

Here, we discuss how the three FGR rates presented in the main text are related to the perturbative expansions discussed above. To simplify the expressions, we assume that the drive is either purely symmetric or purely anti-symmetric about $t = 0$, such that its Fourier coefficients are either all real or all imaginary, and obey $c_{-p}^* = c_p$.

A. Heating rate to second order in λ

First, to obtain a heating rate, we use the Dyson series (S5) for $U_I(t)$ to perturbatively compute the time-dependent expectation of the energy $\langle E \rangle(t)$, where the expectation value is taken in a state that is initially an eigenstate $|i\rangle$ of H_0 . Then

$$\begin{aligned} \langle E \rangle(t) &= \langle i | U_I^\dagger(t) H_0 U_I(t) | i \rangle \\ &= \sum_{n=0}^n \sum_{k=0}^n \langle i | U^{(k)\dagger}(t) H_0 U^{(n-k)}(t) | i \rangle \equiv \sum_{n=0} \langle E \rangle^{(n)}(t) \end{aligned} \quad (\text{S34})$$

To second order in λ , we have:

$$\begin{aligned} \langle E \rangle^{(0)}(t) &= \langle i | H_0 | i \rangle = E_i, \quad \langle E \rangle^{(1)}(t) = \langle i | U^{(1)\dagger}(t) H_0 + H_0 U^{(1)}(t) | i \rangle = 0 \\ \langle E \rangle^{(2)}(t) &= \langle i | U^{(1)\dagger}(t) H_0 U^{(1)}(t) + U^{(2)\dagger}(t) H_0 + H_0 U^{(2)}(t) | i \rangle \\ &= U_{ij}^{(1)\dagger}(t) U_{ji}^{(1)}(t) E_j + 2\Re(U^{(2)}(t))_{ii} E_i \end{aligned} \quad (\text{S35})$$

Note that we have:

$$\begin{aligned} (U^{(1\dagger)})_{ij} U_{ji}^{(1)} &= \lambda^2 \sum_{p_1, p_2} c_{p_1}^* c_{p_2} \sum_j |V_{ij}|^2 \left(\frac{e^{i(\Delta_{ij} - \omega p_1)t} - 1}{(\Delta_{ij} - \omega p_1)} \right) \left(\frac{e^{i(-\Delta_{ij} + \omega p_2)t} - 1}{(-\Delta_{ij} + \omega p_2)} \right) \\ &= -2\lambda^2 \sum_{p_1, p_2} c_{p_1}^* c_{p_2} \sum_j |V_{ij}|^2 \left(\frac{\sin^2(\omega(p_2 - p_1)t/2) - 2\sin^2((\Delta_{ij} - \omega p_1)t/2)}{(\Delta_{ij} - \omega p_1)(\Delta_{ij} - \omega p_2)} \right) \end{aligned}$$

where in the last line, we have used the fact that $c_{p_1}^* c_{p_2} = c_{p_2}^* c_{p_1}$. Using $c_{p_1} = c_{-p_1}^*$, we can re-write this as:

$$(U^{(1\dagger)})_{ij} U_{ji}^{(1)} = 4\lambda^2 \sum_{p_1, p_2} c_{p_1} c_{p_2} \sum_j |V_{ij}|^2 \left(\frac{\sin^2(S_{ij}t/2) - \frac{1}{2}\sin^2(\omega(p_2 + p_1)t/2)}{S_{ij}(\Delta_{ij} - \omega p_2)} \right) \quad (\text{S36})$$

where as above, $S_{ij} = \Delta_{ij} + \omega p_1$. We can simplify the second term in the parentheses by reindexing the sums $p_1 \rightarrow -p_1, p_2 \rightarrow -p_2$ and using our simplifying assumption that $c_{p_1} c_{p_2} = c_{-p_1} c_{-p_2}$.

$$\begin{aligned} \sum_{p_1 \neq -p_2} c_{p_1} c_{p_2} \frac{\sin^2(\omega(p_1 + p_2)t/2)}{\omega(p_1 + p_2)(\Delta_{ij} - \omega p_2)} &= \frac{1}{2} \sum_{p_1 \neq -p_2} \frac{\sin^2(\omega(p_1 + p_2)t/2)}{\omega(p_1 + p_2)} \left(\frac{c_{p_1} c_{p_2}}{\Delta_{ij} - \omega p_2} - \frac{c_{-p_1} c_{-p_2}}{\Delta_{ij} + \omega p_1} \right) \\ &= \frac{1}{2} \sum_{p_1 \neq -p_2} c_{p_1} c_{p_2} \frac{\sin^2(\omega(p_1 + p_2)t/2)}{S_{ij}(\Delta_{ij} - \omega p_2)} \end{aligned} \quad (\text{S37})$$

Thus, we can simplify expression for $\langle E \rangle^{(2)}(t)$ to obtain:

$$\langle E \rangle^{(2)}(t) = \lambda^2 \sum_j |V_{ij}|^2 \sum_{p_1, p_2} c_{p_1} c_{p_2} \left(\frac{2 \sin^2(\omega(p_1 + p_2)t/2) - 4 \sin^2(S_{ij}t/2)}{S_{ij}(\Delta_{ij} - \omega p_2)} \right) (E_i - E_j) \quad (\text{S38})$$

We can extract a single rate from this using the approximations in Fermi's Golden Rule. First, we neglect terms that are rapidly oscillating in time. This leaves only the second sum in parenthesis, and only those terms with S_{ij} very small. Second, at long times, the dominant terms will be those for which both S_{ij} and $\Delta_{ij} - \omega p_2$ are close to vanishing, i.e. terms for which $p_2 = -p_1$ (and hence $\Delta_{ij} - \omega p_2 = S_{ij}$), and $S_{ij} \equiv \Delta_{ij} + \omega p_1 \approx 0$. For these terms, we treat the sincs as approximate delta functions, $\left(\frac{\sin(S_{ij}t/2)}{S_{ij}} \right)^2 \sim \frac{t\pi}{2} \delta(S_{ij})$, to obtain the long-time heating rate:

$$R_i^{\text{heat}} = \frac{d}{dt} \langle E \rangle^{(2)}(t) \Big|_{\text{FGR}} = 2\pi \lambda^2 \sum_p c_p c_{-p} \omega p (\mathcal{A}_i^V(\omega p) - \mathcal{A}_i^V(-\omega p)) \quad (\text{S39})$$

where

$$\mathcal{A}_i^V(\omega) = \sum_j |V_{ij}|^2 \delta(\Delta_{ij} - \omega) \quad (\text{S40})$$

is the spectral function for the operator V at frequency ωp , and the symbol $|_{\text{FGR}}$ means under the assumptions of Fermi's Golden Rule.

For example, for a sine drive of $g(t) = \sin(t)$, this reduces to

$$R_i^{\text{heat}} = \frac{\pi \lambda^2}{2} \omega (\mathcal{A}_i^V(\omega) - \mathcal{A}_i^V(-\omega)) \quad (\text{S41})$$

For the case of the odd box-drive considered in the text, there are only odd-harmonics, and $c_{2n+1} c_{-(2n+1)} = \left(\frac{2}{\pi}\right)^2 \frac{1}{(2n+1)^2}$, yielding

$$R_i^{\text{heat}} = \frac{8\lambda^2}{\pi} \omega \sum_{n=0}^{\infty} \frac{\mathcal{A}_i^V((2n+1)\omega) - \mathcal{A}_i^V(-(2n+1)\omega)}{(2n+1)} \quad (\text{S42})$$

In practice, since \mathcal{A}_i^V decays exponentially in its argument, the matrix elements associated with higher harmonics are strongly suppressed, and the sums are well-described at large frequencies by only including a few harmonics.

B. Fidelity decay rate to second order in λ

The same approach can be used to compute a fidelity decay rate through Fermi's golden rule. To quadratic order in λ , $\log F$ is given by $2\Re(U_{ii}^{(2)})$, and the terms relevant to our rate calculation are exactly as in the heating rate calculation above: only those with $p_2 = -p_1$ and $\Delta_{ij} + \omega p_1 \approx 0$ enter into the Fermi's golden rule rate. Letting $G^{(j)}$ be the j^{th} order contribution to $\log F$, we thus obtain:

$$R_i^{\text{inter}} = \frac{d}{dt} G^{(2)}(t) \Big|_{\text{FGR}} = 2\pi \lambda^2 \sum_{p_1} c_{p_1} c_{-p_1} (\mathcal{A}_i^V(\omega p_1) + \mathcal{A}_i^V(-\omega p_1)) . \quad (\text{S43})$$

For a sine drive, this reduces to

$$R_i^{\text{inter}} = \frac{\pi \lambda^2}{2} (\mathcal{A}_i^V(\omega) + \mathcal{A}_i^V(-\omega)) . \quad (\text{S44})$$

As noted above, for the case of the odd box-drive considered in the text, there are only odd-harmonics, and $c_{2n+1} c_{-(2n+1)} = \left(\frac{2}{\pi}\right)^2 \frac{1}{(2n+1)^2}$; this yields

$$R_i^{\text{inter}} = \frac{8\lambda^2}{\pi} \sum_{n=0}^{\infty} \frac{\mathcal{A}_i^V((2n+1)\omega) + \mathcal{A}_i^V(-(2n+1)\omega)}{(2n+1)^2} \quad (\text{S45})$$

We identify these rates as stemming from interzone processes given that they involve the same matrix elements as and have a similar form to the lowest order heating rate above.

C. Fidelity decay rate to fourth order in λ

As discussed above, at fourth order, the most interesting terms that contribute to the long-time limit are those that do not contribute to heating, and are not suppressed exponentially in ω/J . These terms are given in Eq. (S31). Of the terms listed there, only those in the first line, with $p_3 = -p_4$, contribute to the FGR rate. Using the simplification in Eq. (S32), and the fact that $c_{p_j} c_{-p_j}$ is real, these can be expressed:

$$\begin{aligned} 4\lambda^4 \sum_k \frac{\sin^2(t\Delta_{ik}/2)}{\Delta_{ik}^2} \sum_{j,l} V_{ij} V_{jk} V_{il}^* V_{lk}^* \sum_{p_1, p_3} \frac{c_{p_1} c_{-p_1} c_{p_3} c_{-p_3} \Delta_{jk} \Delta_{kl}}{(\Delta_{jk}^2 - \omega p_1^2)(\Delta_{kl}^2 - \omega p_3^2)} \\ = 4\lambda^4 \sum_k \frac{\sin^2(t\Delta_{ik}/2)}{\Delta_{ik}^2} \left| \sum_{j, p_1 > 0} c_{p_1} c_{-p_1} V_{ij} V_{jk} \frac{2\Delta_{jk}}{\Delta_{jk}^2 - (\omega p_1)^2} \right|^2. \end{aligned} \quad (\text{S46})$$

As above, to obtain a Fermi's Golden rule rate we keep only those terms that do not freeze out until the longest times, and use $\lim_{\Delta_{ik} \rightarrow 0} \left(\frac{\sin(\Delta_{ik} t/2)}{\Delta_{ik}} \right)^2 = \frac{t\pi}{2} \delta(\Delta_{ik})$. For large ω , the matrix elements are strongly suppressed unless $\Delta_{jk} \ll \omega$. Thus up to corrections of order $(\Delta_{jk}/\omega p_1)^2$, we have:

$$R_i^{\text{intra}} = \frac{d}{dt} G^{(4)}(t) \Big|_{\text{FGR}} \approx 2\pi\lambda^4 \left| \sum_{p_1 > 0} \frac{c_{p_1} c_{-p_1}}{(\omega p_1)^2} \right|^2 \sum_k \delta(\Delta_{ik}) \left| \sum_j 2V_{ij} V_{jk} \Delta_{jk} \right|^2 \quad (\text{S47})$$

When Δ_{ik} is close to zero, $2\Delta_{jk} \approx \Delta_{jk} - \Delta_{ij}$, and $\sum_j 2V_{ij} V_{jk} \Delta_{jk} \approx [V, [H_0, V]]_{ik}$. Thus, we obtain:

$$R_i^{\text{intra}} \approx 2\pi\lambda^4 \left| \sum_{p_1 > 0} \frac{c_{p_1} c_{-p_1}}{(\omega p_1)^2} \right|^2 \sum_k \delta(\Delta_{ik}) |\langle i | [V, [H_0, V]] | k \rangle|^2 = \mathcal{A}_i^{[V, [H_0, V]]}(0) \frac{2\pi\lambda^4}{\omega^4} \left| \sum_{p_1 > 0} \frac{c_{p_1} c_{-p_1}}{(p_1)^2} \right|^2 \quad (\text{S48})$$

For a sine drive $g(t) = \sin(t)$, the expression simplifies to

$$R_i^{\text{intra}} \approx \frac{\pi\lambda^4}{8\omega^4} \mathcal{A}_i^{[V, [H_0, V]]}(0) \quad (\text{S49})$$

For the odd box-drive considered in the text, the expression reduces to

$$R_i^{\text{intra}} \approx \frac{\pi^5 \lambda^4}{288\omega^4} \mathcal{A}_i^{[V, [H_0, V]]}(0) \quad (\text{S50})$$

D. Comparison to Floquet-Magnus fidelity decay rate

As one might expect, the dominant fourth-order contribution to the FGR rate matches the rate predicted from a Floquet-Magnus/van Vleck expansion. We now show this explicitly for the odd box drive used in our numerics.

Before discussing the odd box drive, we discuss the even box drive, for which our expressions are somewhat simpler. For an even box drive, $V(t) = V \text{sgn}(\cos(\omega t))$, the Floquet-Magnus expansion up to second order (see, e.g. [2]) gives the effective Hamiltonian:

$$H_F \sim H_0 - \frac{\pi^2 \lambda^2}{24 \omega^2} ([V, [H_0, V]] - [H_0, [H_0, V]]) \quad (\text{S51})$$

From the FGR expression (S43) for $G^{(2)}(t)$ for a constant perturbation, this yields a fidelity decay rate of

$$R_i^{\text{intra}} = \frac{\pi^5 \lambda^4}{288\omega^4} \mathcal{A}_i^{[V, [H_0, V]]}(0) \quad (\text{S52})$$

Note that the $[H_0, [H_0, V]]$ term drops out, since its matrix elements in the H_0 eigenbasis are $(E_i - E_j)^2 V_{ij}$, which vanish for $E_i - E_j = 0$. As a technical note, $[V, [H_0, V]]$ can have a diagonal piece, which we absorb into H_0 , shifting its energies, before running perturbation theory.

We now turn to the odd box drive, $V(t) = V \text{sgn}(\sin(\omega t))$. Physically, it is clear that this should give the same lowest-order rate, though we will see that the derivation is significantly more involved. For an odd drive, the Floquet Magnus expansion up to second order gives the effective Hamiltonian:

$$H_F \sim H_0 - i \frac{\pi}{2} \frac{\lambda}{\omega} [H_0, V] + \frac{\pi^2}{6} \frac{\lambda^2}{\omega^2} [V, [H_0, V]] \quad (\text{S53})$$

Analogously to $[H_0, [H_0, V]]$ above, the $[H_0, V]$ term drops out of the FGR expression for $G^{(2)}(t)$, yielding a contribution of

$$\frac{d}{dt} G^{(4)}(t) \Big|_{\text{FGR}} = \frac{\pi^5 \lambda^4}{18 \omega^4} \mathcal{A}_i^{[V, [H_0, V]]}(0) \quad (\text{S54})$$

However, because $[H_0, V]$ is lower-order in λ and ω relative to the $[V, [H_0, V]]$ term, fourth-order TDPT for a quench causes it to enter on the same footing as second order TDPT on $[V, [H_0, V]]$.

For a quench, fourth-order TDPT for a perturbation $\frac{\pi}{2} \frac{\lambda}{\omega} [H_0, V]$ yields (note that $[H_0, V]_{ij} = (E_j - E_i) V_{ij} = \Delta_{ij} V_{ij}$)

$$\Re \left(\langle i | U_I^{(4)} | i \rangle \right) = \frac{\pi^4 \lambda^4}{8 \omega^4} \sum_{jkl} V_{ij} V_{jk} V_{kl} V_{li} \Delta_{ij} \Delta_{jk} \Delta_{kl} \Delta_{li} \left(\frac{\sin^2(\Delta_{ij} t/2)}{\Delta_{ij}^2 \Delta_{kj} \Delta_{lj}} + \frac{\sin^2(\Delta_{ik} t/2)}{\Delta_{ik}^2 \Delta_{jk} \Delta_{lk}} + \frac{\sin^2(\Delta_{il} t/2)}{\Delta_{il}^2 \Delta_{jl} \Delta_{kl}} \right) \quad (\text{S55})$$

The first and third terms in the parentheses contribute to the late-time behavior when Δ_{ij} and Δ_{il} are close to zero; however, these contributions are completely suppressed from the factors of Δ_{ij} and Δ_{il} from the matrix elements of $[H_0, V]$ appearing in the pre-factor. The dominant term at late times is thus proportional to

$$\sum_{jkl} V_{ij} V_{jk} V_{kl} V_{li} \frac{\sin^2(\Delta_{ik} t/2)}{\Delta_{ik}^2} \Delta_{il} \Delta_{ij} = \sum_k \frac{\sin^2(\Delta_{ik} t/2)}{\Delta_{ik}^2} \left| \sum_j V_{ij} V_{jk} \Delta_{ij} \right|^2 \quad (\text{S56})$$

When Δ_{ik} is close to zero, $\Delta_{ij} \approx -\frac{1}{2}(\Delta_{jk} - \Delta_{ij})$, and so $\sum_j V_{ij} V_{jk} \Delta_{ij} \approx -\frac{1}{2} [V, [H_0, V]]_{ik}$. Treating the sinc as proportional to a delta function as before, we have a contribution of

$$\frac{d}{dt} G^{(4)}(t) \Big|_{\text{FGR}} \sim \frac{\pi^5 \lambda^4}{32 \omega^4} \mathcal{A}_i^{[V, [H_0, V]]}(0) \quad (\text{S57})$$

We also have a contribution from $G^{(3)}$ which stems from cross-terms between the $[H_0, V]$ and $[V, [H_0, V]]$ terms. We have, taking V real for simplicity, and keeping only terms of the relevant order in $\frac{\lambda}{\omega}$,

$$\Re \left(\langle i | U_I^{(3)} | i \rangle \right) = \frac{\pi^4 \lambda^4}{12 \omega^4} \sum_{jk} \left(\frac{\sin^2(\Delta_{ij} t/2)}{\Delta_{ij}^2 \Delta_{kj}} + \frac{\sin^2(\Delta_{ik} t/2)}{\Delta_{ik}^2 \Delta_{jk}} \right) \left(\Delta_{ij} \Delta_{jk} V_{ij} V_{jk} [V, [H_0, V]]_{ki} + \Delta_{jk} \Delta_{ki} [V, [H_0, V]]_{ij} V_{jk} V_{ki} + \Delta_{ij} \Delta_{ki} V_{ij} [V, [H_0, V]]_{jk} V_{ki} \right) \quad (\text{S58})$$

Through relabeling of $j \leftrightarrow k$, this becomes

$$\Re \left(\langle i | U_I^{(3)} | i \rangle \right) = \frac{\pi^4 \lambda^4}{6 \omega^4} \sum_{jk} \frac{\sin^2(\Delta_{ik} t/2)}{\Delta_{ik}^2 \Delta_{jk}} \left(\Delta_{ik} \Delta_{kj} [V, [H_0, V]]_{ij} V_{jk} V_{ki} + \Delta_{kj} \Delta_{ji} V_{ij} V_{jk} [V, [H_0, V]]_{ki} + \Delta_{ik} \Delta_{ji} V_{ij} [V, [H_0, V]]_{jk} V_{ki} \right) \quad (\text{S59})$$

Note that the late-time contribution of the sinc term comes from Δ_{ik} close to 0, which eliminates the first and last terms in the parentheses under Fermi's Golden Rule. That is, our late-time behavior is determined by the middle term,

$$\begin{aligned} \Re \left(\langle i | U_I^{(3)} | i \rangle \right) \Big|_{\text{FGR}} &= \frac{\pi^4 \lambda^4}{6 \omega^4} \sum_{jk} \frac{\sin^2(\Delta_{ik} t/2)}{\Delta_{ik}^2 \Delta_{jk}} \left(\Delta_{kj} \Delta_{ji} V_{ij} V_{jk} [V, [H_0, V]]_{ki} \right) \\ &= \frac{\pi^4 \lambda^4}{6 \omega^4} \sum_k [V, [H_0, V]]_{ik} \frac{\sin^2(\Delta_{ik} t/2)}{\Delta_{ik}^2} \sum_j \Delta_{ij} V_{ij} V_{jk} \end{aligned} \quad (\text{S60})$$

When Δ_{ik} is close to zero, $\Delta_{ij} \approx -\frac{1}{2}(\Delta_{jk} - \Delta_{ij})$, and so $\sum_j V_{ij}V_{jk}\Delta_{ij} \approx -\frac{1}{2}[V, [H_0, V]]_{ik}$, so we have, under the FGR assumptions,

$$\Re \left(\langle i | U_I^{(3)} | i \rangle \right) |_{\text{FGR}} \approx -\frac{\pi^4 \lambda^4}{12\omega^4} \sum_k |[V, [H_0, V]]_{ik}|^2 \frac{\sin^2(\Delta_{ik}t/2)}{\Delta_{ik}^2} \quad (\text{S61})$$

and

$$\frac{d}{dt} G^{(3)}(t) |_{\text{FGR}} = -\frac{\pi^5 \lambda^4}{12\omega^4} \mathcal{A}_i^{[V, [H_0, V]]} \quad (\text{S62})$$

Putting together the three contributions, we have a rate

$$R_i^{\text{intra}} = \frac{\pi^5 \lambda^4}{\omega^4} \mathcal{A}_i^{[V, [H_0, V]]}(0) \left(\frac{1}{18} + \frac{1}{32} - \frac{1}{12} \right) = \frac{\pi^5 \lambda^4}{288\omega^4} \mathcal{A}_i^{[V, [H_0, V]]}(0) \quad (\text{S63})$$

This rate for the odd drive matches that of the even drive.

E. Crossover frequency

In this section, we approximate the crossover frequency where the intrazone rate begins to dominate the interzone rate. We assume that the crossover ω_c occurs at a value of ω that is either comparable to or larger than the local energy scale J of H_0 ; as we will see below, this occurs when λ is small relative to J . For simplicity, we consider the sinusoidal drive with $g(t) = \sin(t)$, but the crossover frequency for a general drive will have the same parametric dependence on the energy scales λ and J . The intrazone and interzone rates for this drive are

$$R_i^{\text{intra}} = \frac{\pi \lambda^4}{8\omega^4} \mathcal{A}_i^{[V, [H_0, V]]}(0) \quad (\text{S64})$$

$$R_i^{\text{inter}} = \frac{\pi \lambda^2}{2} (\mathcal{A}_i^V(\omega) + \mathcal{A}_i^V(-\omega)) \sim \pi \lambda^2 a_i^V e^{-\omega/J} \quad (\text{S65})$$

In the above asymptotic expression for the interzone rate, we used the fact noted in the main text that $\mathcal{A}_i^V(\omega)$ decays exponentially with frequency [3]. We wrote the asymptotic proportionality constant between $\mathcal{A}_i^V(\omega)$ and $e^{-\omega/J}$ as a_i^V , and we expect this constant to be approximated by or strongly correlated with $\mathcal{A}_i^V(0)$. Setting the asymptotic expressions equal to one another yields

$$\left(\frac{\omega}{J} \right)^4 e^{-\omega/J} = \frac{\lambda^2 \mathcal{A}_i^{[V, [H_0, V]]}(0)}{8J^4 a_i^V} \quad (\text{S66})$$

The crossover frequency is the largest ω solution to this, above which the intrazone rate dominates. This is equivalent to solving the problem

$$x^4 e^{-x} = k \quad (\text{S67})$$

for the largest solution. Solving via iteration yields

$$\begin{aligned} x &\sim \log\left(\frac{1}{k}\right) + 4 \log\left(\log\left(\frac{1}{k}\right)\right) \\ e^{-x} &\sim \frac{k}{\log\left(\frac{1}{k}\right)^4} \end{aligned} \quad (\text{S68})$$

so we have that the crossover frequency ω_i^c is

$$\omega_i^c \sim J \log \left(\frac{8J^4 a_i^V}{\lambda^2 \mathcal{A}_i^{[V, [H_0, V]]}(0)} \right) \quad (\text{S69})$$

and the rate R_i^c at the crossover is

$$R_i^c \sim \frac{\pi \lambda^4 \mathcal{A}_i^{[V, [H_0, V]]}(0)}{8J^4 \log \left(\frac{8J^4 a_i^V}{\lambda^2 \mathcal{A}_i^{[V, [H_0, V]]}(0)} \right)^4} \quad (\text{S70})$$

Note that H_0 implicitly contains a factor of J , and the averaging in the spectral function implicitly yields an inverse factor of J , so we have that $a_i^V \sim L^d/J$ and $\mathcal{A}_i^{[V, [H_0, V]]}(0) \sim L^d J$. Neglecting $O(1)$ factors, the dominant dependence on J and λ are through $\omega_i^c \sim J \log(J^2/\lambda^2) \sim J \log(J/\lambda)$ and $R_i^c \sim L^d J \frac{(\lambda/J)^4}{\log(J/\lambda)^4}$ at small λ . Note that there are $O(1)$ factors that depend on the details of the state, V , and H_0 through the relative magnitude of off-diagonal matrix elements of V and $[V, [H_0, V]]$.

In one dimension, spectral functions of local operators decay weakly superexponentially in the frequency ω [3]; this only changes the results above by multiplicative factors of $\log(\log(J/\lambda))$.

[1] Ronald Forrest Fox, “Critique of the generalized cumulant expansion method,” *Journal of Mathematical Physics* **17**, 1148–1153 (2008).

[2] Tomotaka Kuwahara, Takashi Mori, and Keiji Saito, “Floquet-magnus theory and generic transient dynamics in periodically driven many-body quantum systems,” *Annals of Physics* **367**, 96–124 (2016).

[3] Dmitry A. Abanin, Wojciech De Roeck, and Francois Huveneers, “Exponentially slow heating in periodically driven many-body systems,” *Phys. Rev. Lett.* **115**, 256803 (2015).